Open-slope, translational submarine landslide in a tectonically active volcanic continental margin (Licosa submarine landslide, southern Tyrrhenian Sea)

M. SAMMARTINI[1,2], A. CAMERLENGHI[1]*, F. BUDILLON[3], D. D. INSINGA[3], F. ZGUR[1], A. CONFORTI[3], M. IORIO[3], R. ROMEO[1] & R. TONIELLI[3]

[1]*National Institute of Oceanography and Applied Geophysics (OGS), Borgo Grotta Gigante 42/c, 34010 Sgonico, Trieste, Italy*

[2]*Marine Geology & Seafloor Surveying, Department of Geosciences, University of Malta, Msida, Malta*

[3]*Institute for Coastal Marine Environment (IAMC), National Research Council of Italy (CNR), Calata Porta di Massa, Porto di Napoli, 80133 Naples, Italy*

M.S., 0000-0003-1338-5475; A.C., 0000-0002-8128-9533

Present address: M.S., Institut für Geologie, Leopold-Franzens-Universität Innsbruck, Innrain 52f, A-6020 Innsbruck, Austria

**Correspondence:* *acamerlenghi@inogs.it*

Abstract: The southern Tyrrhenian continental margin is the product of Pliocene–Recent back-arc extension. An area of approximately 30 km^2 of gentle (about 1.5°) lower slope of the last glacial outer shelf sedimentary wedge in water depths of between 200 and 300 m failed between 14 and 11 ka BP. We approached the landslide by multibeam and sub-bottom profiler surveying, high-resolution multichannel seismics, and coring for stratigraphic and geotechnical purposes. With regard to a slope-stability analysis, we carried out an assessment of the stratigraphic and structural setting of the area of the Licosa landslide. This analysis revealed that the landslide detached along a marker bed that was composed of the tephra layer Y-5 (*c.* 39 ka). Several previously unknown geological characteristics of the area are likely to have affected the slope stability. These are the basal erosion of the slope in the Licosa Channel, a high sedimentation rate in the sedimentary wedge, earthquake shaking, the volcanic ash nature of the detachment surface, subsurface gas/fluid migration, and lateral porewater flow from the depocentre of wedge to the base of the slope along the high-permeability ash layers. A newly discovered prominent structural discontinuity is identified as the fault whose activity may have triggered the landslide.

Modern submarine landsides often occur, paradoxically, in areas of the seafloor where morphological and geological characteristics suggest gravitational stability. The observation of the distribution of submarine landslides in sedimentary basins indicates clearly that they can be found on tectonically active and inactive margins, in areas of high sedimentation rate, as well as in sediment-starved areas, on steep and gentle slopes (e.g. Urgeles & Camerlenghi 2013). In order to identify the causes of submarine slope failure, several factors must be considered among those that decrease stability (preconditioning factors, depending on sedimentology, fluid-flow regime and tectonic history) and those that ultimately initiate the failure (triggering factors, often associated with events such as ground shaking, slope basal erosion, gas emissions and storms) (e.g. Lee *et al.* 2007).

The Campanian margin in the southern Tyrrhenian Sea is deeply incised by submarine canyons with steep slopes (Milia 2000; D'Argenio *et al.* 2004; Budillon *et al.* 2011). At least eight translational landslides have been identified in the bathymetric range between 200 and 700 m (Fig. 1) (Bellonia *et al.* 2008; Budillon *et al.* 2014). Among these, the Licosa submarine landslide, originally identified and described by Trincardi & Field (1992), is located between 200 and 300 m water depth just seawards of the shelf break (Fig. 1). It affected an area of the seafloor of about 30 km^2, on the seawards termination

From: Lintern, D. G., Mosher, D. C., Moscardelli, L. G., Bobrowsky, P. T., Campbell, C., Chaytor, J. D., Clague, J. J., Georgiopoulou, A., Lajeunesse, P., Normandeau, A., Piper, D. J. W., Scherwath, M., Stacey, C. & Turmel, D. (eds) 2019. *Subaqueous Mass Movements*. Geological Society, London, Special Publications, **477**, 133–150.
First published online May 24, 2018, https://doi.org/10.1144/SP477.34

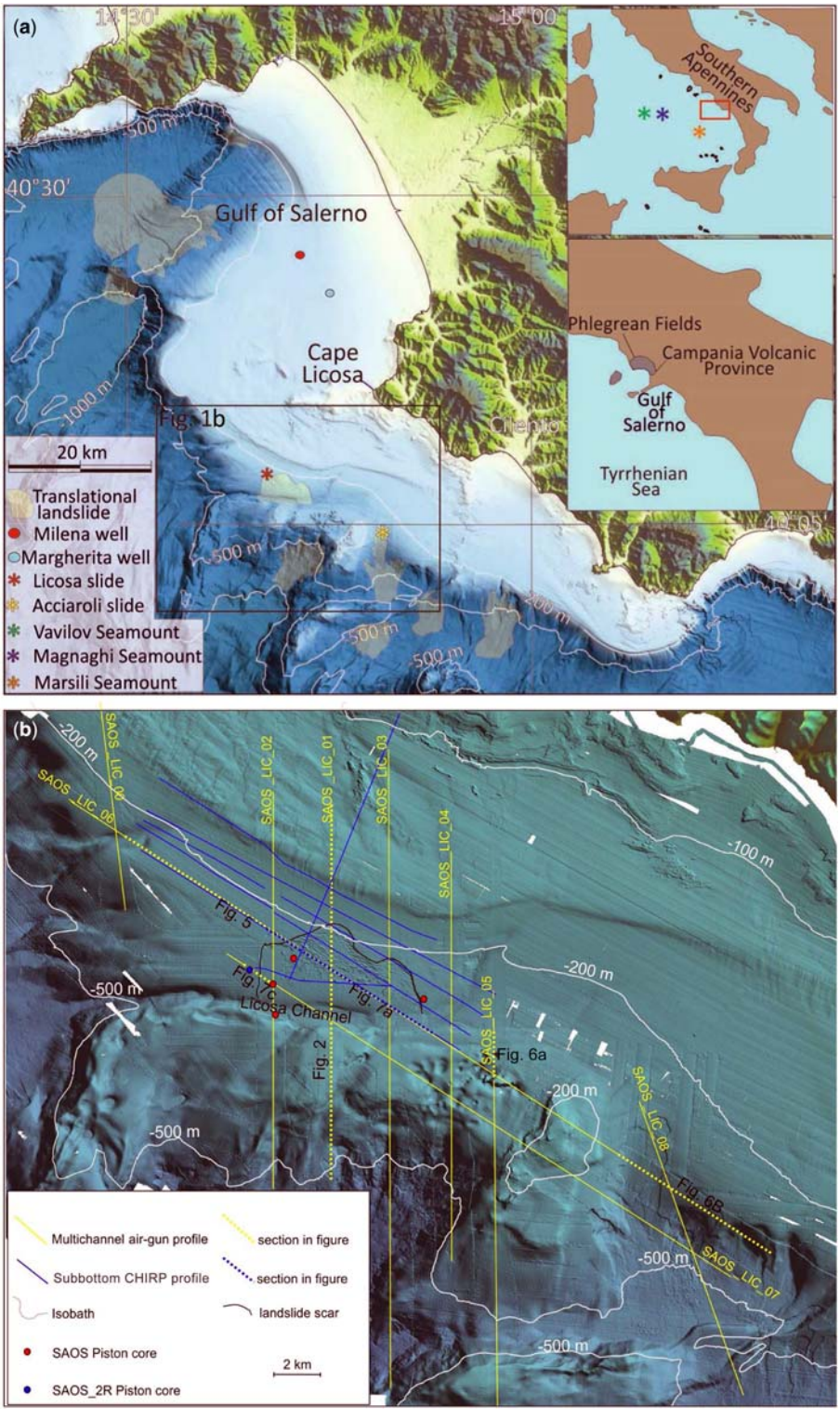

of a last glacial lowstand sedimentary wedge. The detachment scar is 6 km long, the maximum height of the missing sedimentary section is about 7.5 m, and the estimated volume of removed sediment is between 0.5 and 0.8 km^3 (after Trincardi & Field 1992 and Trincardi *et al.* 2003). The sediment collapse has retrogressed upslope, leaving an area of remnant sedimentary blocks close to the scar. The slip plane is a smooth and continuous surface dipping seawards by about 1.5°–3°, probably exposed after the failure as a result of complete mobilization of sediments above it. It is now covered by about 65 cm of post-slide sedimentary drape (Iorio *et al.* 2014).

The landslide has been dated about 14 ka cal BP by Trincardi *et al.* (2003), who suggested a failure by a sudden increase in porewater pressure induced by rapid global sea-level rise (Meltwater Pulse 1A) on a slope preconditioned to failure by high sedimentation rates during the growth of the lowstand sedimentary wedge. Earthquake shaking was considered as a possible external trigger of the landslide. The age of the slide was determined based on micropalaeontological determinations that showed an incomplete lower portion of Greenland Interstadial (GI) 1 at the base of the post-slide drape. Iorio *et al.* (2014) refined the age of the landslide, which was assessed at 11 cal ka based on the erosional hiatus that is present seawards of the landslide area. The hiatus extends from 21 to 11 cal ka, as inferred by a palaeomagnetic secular variation model, tephrochronology and radiometric dating.

Several open questions were left after the initial assessment of the landslide: Is rapid sea-level rise the only preconditioning factor involved in decreasing the sediment shear strength? Does the age refinement introduced by Iorio *et al.* (2014) impose the identification of alternative factors? What is the role of widespread and often thick ash layers in the slope stability? Is there a fluid-flow component relevant to the slope stability? And, finally, where is the source of ground shaking capable of triggering a landslide?

In the framework of the project RITMARE, we approached the Licosa submarine landslide with the purpose of identifying evidence in the regional geological structure, for potential slope-failure preconditioning factors and triggering factors. This manuscript presents the results of high-resolution seismostratigraphic analysis and part of the lithological data.

Regional geological setting

The Tyrrhenian back-arc basin evolved since the Tortonian as a consequence of the ESE migration of the Apennines–Calabrian subduction system (Malinverno & Ryan 1986; Faccenna *et al.* 2001). The opening of the basin, initially affecting the Sardinia margin, focused on the Central and Southern Tyrrhenian sectors in the Pliocene and Pleistocene due to the SE migration of the Calabrian subduction front (Faccenna *et al.* 2001). The Campanian margin, floored by rifted continental crust, is tectonically active (e.g. Mattei *et al.* 2002). The main opening of the basin was dominated by a strike-slip regime that caused large vertical displacements on the margin along north–south- to NW–SE-trending faults, included thrusting and folding. In the Early Pleistocene, extension created horst-and-graben structures trending NE–SW that characterize the margin structure today. The current extension, active since the Middle Pleistocene, is believed to be trending NE–SW (the fourth deformation event of Caiazzo *et al.* 2006).

According to Prada *et al.* (2014), lithospheric extension produced basaltic back-arc magmatic crust at the transition to the extended continental crust, while exhumed serpentinized mantle with basaltic intrusion occur below the deepest abyssal plains. The Tyrrhenian Sea opening was accompanied by a 12 Ma–Present intraplate and arc-type volcanism, generating Vavilov, Magnaghi and Marsili seamounts – volcanic edifices in the newly-formed abyssal plains. The Campanian volcanic province, adjacent to the study area, has developed since 0.2 Ma with shoshonitic, potassic and ultra-potassic volcanic eruptions that involved phenomena of explosive activity and caldera collapse (Peccerillo 2016).

Methods

The data used in this study include bathymetric data, multichannel seismic profiles and sub-bottom CHIRP-Sonar profiles acquired onboard the R/V *Urania* during the SAOS 2014 cruise.

The multibeam bathymetric data acquired with the hull-mounted Kongsberg EM 710 were processed to provide a 10 × 10 m DEM grid of the area. The instrument operating frequency was set to 100 kHz and the maximum swath width was 150°, generating 800 beams for each ping.

Fig. 1. (**a**) Location of the continental margin off the Campania region in the southern Tyrrhenian Sea. Note that at least eight translational landslide systems, larger than 15 km^2, are located on this margin. These landslides include the Licosa landslide, the focus of this study, and the Acciaroli landslide. The map locates the boreholes used for stratigraphic ties. (**b**) Location of the newly collected sediment cores, and the multichannel seismic and sub-bottom profiles.

The multibeam bathymetric dataset that was acquired using the Reason Seabat 8111 and Reson Seabat 8150 systems, onboard R/V *Explora* during the LICOSA 2013 cruise, was used to improve imaging of the seafloor in the landslide area. The complete bathymetric base map of the Campania margin (Fig. 1) was compiled with data acquired by IAMC CNR between 2002 and 2010.

Sub-bottom profiles were acquired along the track of multichannel seismics using a hull-mounted DATASONIC CHIRP III CAP6600. The source signal was a FM-swept pulse with a frequency band of 2–7 kHz and the rate was in a time range between 0.750 and 1.5 s. This frequency band provides submetre vertical resolution, and the ping rate provides horizontal sampling of between 1.4 and 3 m (at 6.85 km/h ship speed, equivalent to 3.7 knots).

The multichannel seismic reflection acquisition was carried out using the OGS system composed of a single 1 l Sercel-Sodera Mini GI (generator–injector) gun fired in harmonic mode (30 G + 30 I). The shot point distance and the record length were set, respectively, to 9.375 m and 3 s. The source was towed at a depth of 1.5 m and at a velocity of 6.8 km/h. The OGS 96-channel, 300 m-long Geometrics Geoeel digital streamer was the receiving system. The streamer was towed at a depth of 0.5–1 m below the sea surface. The seismic system provided a maximum fold coverage of 16 traces for common depth point (CDP) and an effective trace distance in the stacked section of 1.56 m.

Sediment cores taken within and outside the landslide scar (Fig. 1b) were obtained using the Carma® piston corer (PC) (Magagnoli 2017) with variable weight (from 1250 to 1850 kg) and pipe length (the best penetration was obtained with 15 m-long pipes). Core SAOS-2R was retrieved in 300 m water depth, 5.25 km seawards of the continental shelf edge and about 290 m westwards of the lateral headwall of the landslide scar (WGS84: latitude and longitude of 40° 7.927′ N, 14° 43.165′ E). It displays a 9.02 m-thick sedimentary succession (core shortening is not considered) that is Late Pleistocene–Holocene in age (Trincardi *et al.* 2003; Iorio *et al.* 2014).

Tephra samples were disaggregated in water, and were wet sieved through 500, 250, 125, 90 and 63 μm meshes. They were observed under a binocular microscope for lithological description, and the glass fraction (pumice and shards) was handpicked for chemical analyses. Glass concentrates were obtained avoiding samples with vesicles, crystalline intergrowth and alteration. Selected grains then were rinsed in distilled water, cleaned with an ultrasonic probe and mounted on epoxy resin. They were individually analysed for major elements, using an Oxford Instruments Microanalysis Unit equipped with an INCA X-act detector and a JEOL JSM-5310 SEM (scanning electron microscope) at DiSTAR (University of Naples Federico II). The analytical procedures are reported in detail in Margaritelli *et al.* (2016).

Depths and unit thickness estimations in seismic profiles have been obtained by assuming likely compressional velocity (V_p) values for the sediment composition and lithology extrapolated by the knowledge of the regional geology. The average velocity used in the sedimentary units containing the landslide and immediately below is 1700 m s^{-1}, corresponding to moderately compacted (bulk sediment density 1.8 g cm^{-3}) siliciclastic sediments (e.g. Hamilton 1978). The thickness of the lowstand sedimentary wedge, from which lower slope the landslide was detached, has been calculated using a range of velocities (1500–1700 m s^{-1}) to produce maximum and minimum thickness values. The velocity of 1500 m s^{-1}, typical of seawater, has been considered to take into account the possibility of sediment underconsolidation, yielding little porosity decrease with depth in the high sedimentation rate in the sedimentary wedge (see the Discussion). The average velocity of the entire sedimentary sequence overlying the substratum has been assumed to be equal to 2000 m s^{-1}, assuming an average density of 2 g cm^{-3} (after Hamilton 1978).

The thickness maps of the wedge and the landslide deposit have been generated using both multichannel seismic profiles and sub-bottom profiles. For the wedge thickness map, a grid of 20 × 20 m has been used. The deposit thickness map was created using a grid of 100 × 20 m with some additional control points that were added manually due to low seismic coverage in the east–west direction.

Results

The landslide scarp is a *c.* 7.5 m-high seafloor step located approximately 2 km seawards of the continental shelf break (Fig. 1). Downslope of the scarp is the transition zone, characterized by the presence of remnant sedimentary blocks and by a smooth seafloor surface further downslope. The blocks are elongated parallel to the slope strike and have dimensions of up to a few hundreds of metres close to the scarp. The slope gradient increases progressively downslope within the transition zone. The seafloor morphology and the seismic reflection record show that the east–west-orientated Licosa Channel is a zone where the landslide deposit has accumulated (Figs 2 & 3).

The seismic reflection data (Fig. 2) show an irregular, seawards-dipping, high-amplitude reflection seismic unit that acts as substratum. Below the landslide, such a unit is located between 275 and 1000 ms (two-way travel time (TWTT)), which corresponds, assuming an average seismic velocity of 2000 m s^{-1}, to 275 and 1000 m, respectively.

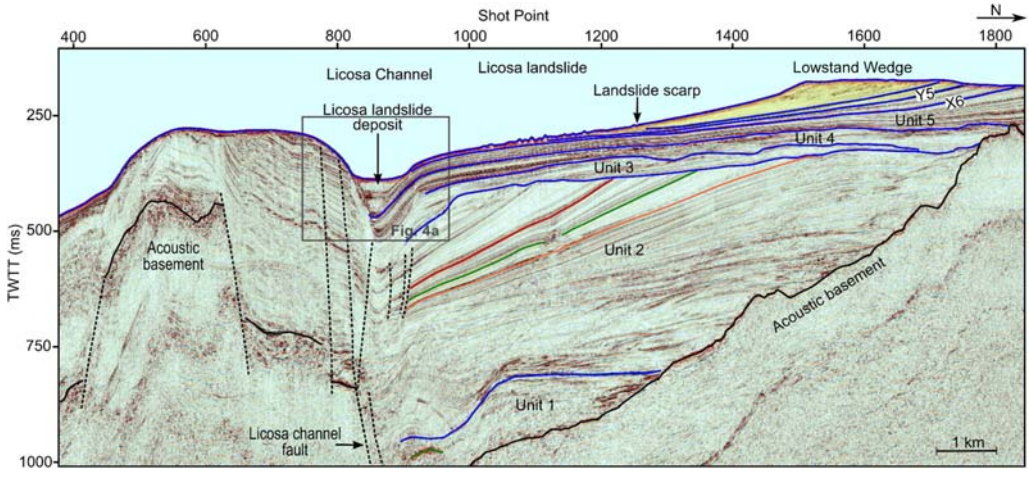

Fig. 2. Multichannel seismic profile LIC_01 across the Licosa landslide shows the subseafloor seismic stratigraphy and the main structural discontinuities. The substratum is overlain by a thick aggradational sedimentary succession, within which five main seismic units were identified based on prominent unconformities. The lowstand wedge, north of the landslide scarp, is highlighted in yellow. Three prominent reflections within Unit 5 have been identified. Two of them have been correlated to tephra layers: Campanian Ignimbrite Y-5 (39 ka) and tephra X-6 (109 ka BP). Vertical exaggeration is ×8.5. The location of the profile is shown in Figure 1b.

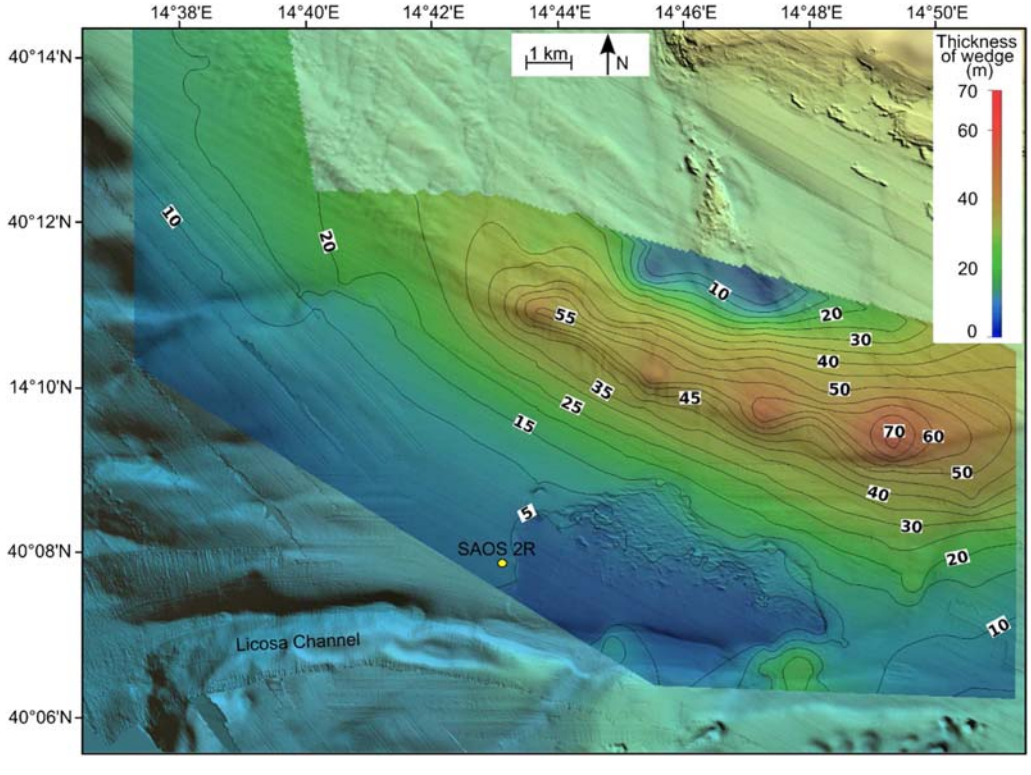

Fig. 3. Bathymetric image of the Licosa landslide area with an isopach map of the lowstand wedge, north of the landslide scarp. The isopach lines identify the thickness in metres obtained considering Y-5 as the base layer of the wedge and assuming a constant velocity of 1700 m s^{-1}.

The substratum is unconformably overlain by a thick aggradational sedimentary succession exceeding 600 ms (TWTT) in thickness in our seismic data (600 m assuming an average seismic velocity of 2000 m s^{-1}). Prominent unconformities allow identification of five main seismic units (Fig. 2). The deepest Unit 1 is wedge shaped and terraced with onlap/downlap lateral terminations on the substratum. Unit 2 includes a 20 km-wide, lateral aggrading and prograding succession characterized by high-amplitude continuous reflections sub-parallel to the divergent geometry. The unit is bounded at the top by a wide erosional surface.

Above Unit 2 are three sedimentary sequences, each bounded at the top by an erosional surface. Unit 5 is represented by a sedimentary wedge as thick as 150 ms (TWTT) (less than 150 m).

The Licosa Channel (Fig. 2) is located just 3 km south of the landslide scarp and, in its western part, represents an important geological discontinuity. The channel is emplaced along a major subvertical fault system about 14 km long in an east–west direction, which makes it difficult to correlate the seismostratigraphic units south of the Licosa Channel to the five units identified to the north of the Licosa landslide. Only the acoustic substratum is univocally identified and is displaced in several places by subvertical faults.

The seismic record in the Licosa Channel is characterized by the presence of two acoustically transparent channel-filling deposits separated by high-amplitude sub-parallel reflections (Fig. 4a). The upper one has a horizontal extension of 600 m and reaches a maximum thickness of 30 ms (TWTT) in the LIC_01 profile (25.5 m assuming a constant velocity of 1700 m s^{-1}) (Fig. 4b). The lower transparent unit, with a maximum horizontal extension of 220 m and a maximum thickness of 20 ms (TWTT) (17 m assuming a constant velocity of 1700 m s^{-1}), is significantly smaller than the upper deposit. The lower unit thins and pinches out in the easternmost sector of the channel.

Multiple and adjacent cone-shaped seabed depressions that we interpret as buried pockmarks are imaged in multichannel seismic profile LIC_06, approximately 2 km NW of the slide scar (Fig. 5). These pockmarks are layer-bound within Unit 2 and reach a maximum vertical extent of about 75 m (considering a constant velocity of 1700 m s^{-1}), with a typical width of 60–100 m from shoulder to shoulder. Although the fluid conduits below the pockmarks are not clearly visible on the seismic profile, some anomalous amplitudes and some acoustic masking can be detected underneath the biggest ones. The same area is characterized by the presence of subvertical, small-offset normal faults that do not extend above the erosional surface at the base of Unit 5. More evidence of fluid escape is present 15 km SE of the landslide in the same line LIC_06. Here, anomalous high amplitudes and upwards concavity are affecting the same layer interval that hosts the buried pockmarks (Fig. 6a, b). Furthermore, recent fluid-escape activity is highlighted by the presence of a superficial pockmark SE of the Licosa landslide (Fig. 6a). The pockmark, with a diameter of 130 m and depth of about 55 m, is visible on both seismic data and bathymetric grid.

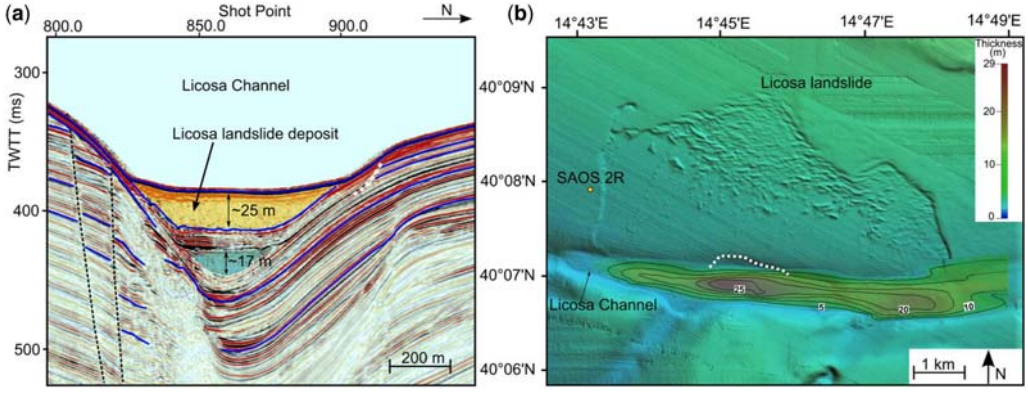

Fig. 4. Seismic section and isopach map of the Licosa landslide deposit. (**a**) Multichannel seismic profile LIC_01 in the Licosa Channel shows the presence of two acoustically transparent seismic units. The Licosa landslide deposit is highlighted in yellow. The deeper units, thought to be an older landslide, are highlighted in blue. The location of the profile is shown in Figure 2. Vertical exaggeration is ×6. (**b**) Isopach map of the Licosa landslide deposit. The isopach lines show the thickness of the deposit in metres, calculated assuming a constant velocity of 1700 m s^{-1}. The maximum thickness (25.5 m) is reached along multichannel seismic profile LIC_01. For the names of the seismic lines and cores see Figure 2.

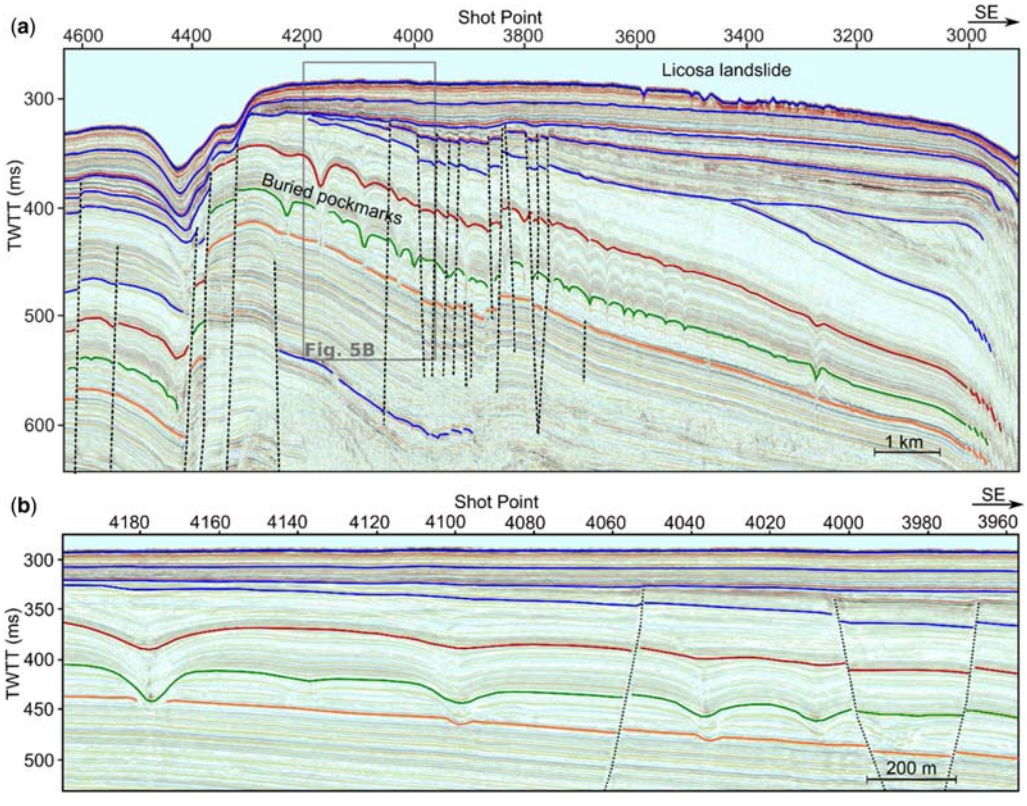

Fig. 5. (**a**) Buried pockmark identified on the multichannel seismic profile LIC_06, approximately 2 km NW of the slide scar. In the same area, subvertical normal faults, likely to be part of a polygonal fault system, are present. Vertical exaggeration is ×24. (**b**) Zoom of the buried pockmark. The location of the seismic profile is shown in Figure 1b. Vertical exaggeration is ×3.

A buried landslide that caused mobilization of sediment in a SW direction is identified at shallow depth (*c.* 50 ms TWTT below the seafloor, corresponding to *c.* 40 m) in profile LIC 06 (dashed line in Fig. 6b). The buried scar of this landslide has a horizontal extent of about 2 km and seems to have been caused by lateral detachment and translation of a sedimentary section without complete evacuation of the landslide translation zone. This buried landslide is located stratigraphically below the Acciaroli landslide (Fig. 1: see also Bellonia *et al.* 2008), which retains a prominent expression in the present-day seafloor morphology.

Approximately 250 m stratigraphically below the Acciaroli landslide, chaotic, high-amplitude reflections have been interpreted as an additional possible landslide deposit (Fig. 6b). In this case, the landslide occurred from the structural high that is visible NW of the area. It is characterized by a horizontal extent and vertical uplift of about 800 and 20 m, respectively. The lack of seismic profiles in this area has not allowed 3D imaging of the two features.

The sedimentary record in core SAOS-2R is made up of sandy mud deposits and, secondarily, muddy sand deposits; the coarse fraction is composed of bioclasts, pumice, scoriae and lithoclasts. The coarser beds occur mostly between 40–60, 148–160, 360–400, 705–740 and 780–902 cm bsf (below seafloor) (dashed lines in Fig. 7b). According to Iorio *et al.* (2014), the base of the post-slide drape does not exceed a depth of 60–65 cm bsf; the limited thickness of this sedimentary drape is in agreement with the lack of a distinguishable drape unit in the high-resolution seismic records due to resolution limitation (Fig. 7c).

Three primary tephra layers have been identified by visual inspection in core SAOS-2R. They are located at 267 and 372 cm bsf, and at the core bottom (Fig. 7).

- Tephra SAOS2R-267 – 2 cm-thick coarse-grained ash made of angular to sub-angular light grey pumice with elongated vesicles. Fibrous glass shards and loose crystals of K-feldspar fully occur.

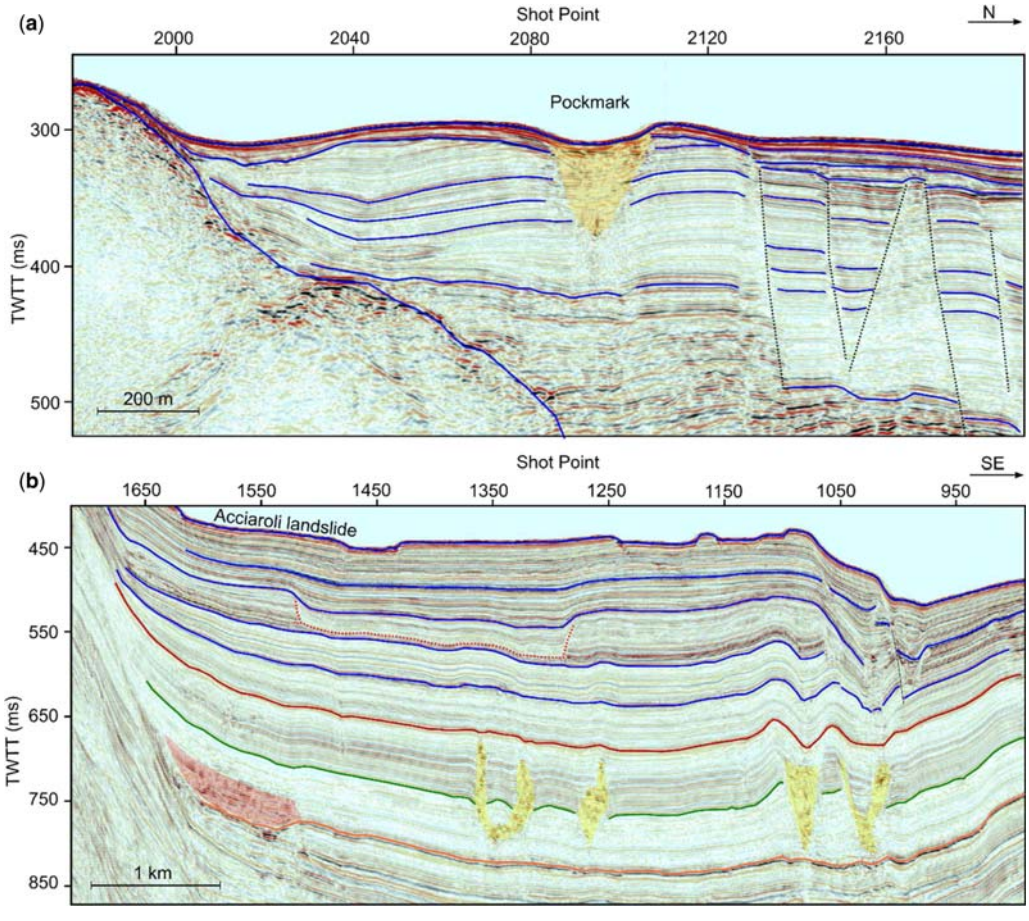

Fig. 6. More evidence of fluid escape appears within 15 km SE of the landslide, along multichannel seismic profile LIC_05 and LIC_6. (**a**) The presence of a surficial pockmark indicates recent fluid-escape activity. The pockmark is visible both on the seismic data (multichannel seismic profile LIC_05) and the bathymetric grid. Vertical exaggeration is ×3.8. (**b**) The image (multichannel seismic profile LIC_06) shows in yellow the presence of anomalous high-amplitude and concave-upwards signals, which affect the same layer interval hosting the buried pockmark (Fig. 5). A buried landslide scar is identified, with a dashed line, at a depth of approximately 40 m. An additional landslide deposit, at a depth of approximately 250 m, is highlighted in red. Vertical exaggeration is ×9. The location of both seismic profiles is shown in Figure 1b.

- Tephra SAOS2R-372 – *c.* 17 cm thick and is represented at its bottom by a 2 cm-thick coarse-grained ash made of sub-angular light and dark grey pumice with low and elongated vesicles, blocky glass shards, and loose crystals of K-feldspar and clinopyroxene. This interval sharply passes upward to a *c.* 15 cm-thick deposit containing accretionary lapilli embedded in silty matrix made of volcanic components (micropumice, glass shards with thin-walled and bubble-wall junction morphologies, and loose crystals of K-feldspar, clinopyroxene and biotite).
- Tephra SAOS2R-bottom – coarse-grained ash embedded in silty matrix. The ash is made of light and dark grey pumice with elongated vesicles, glass shards with bubble-wall and blocky morphologies, and loose crystals of K-feldspar. Some lithic fragments are also present.

According to the total alkali/silica (TAS) classification diagram (Le Maitre 2005), the tephras have trachyphonolitic (SAOS2R-bottom and SAOS2R-372) and trachytic (SAOS2R-267) compositions (Fig. 7; Table 1) that are typical of the mildly silica–undersaturated potassic series erupted at the Campania Plain during the Late Pleistocene–Holocene (Pabst *et al.* 2008).

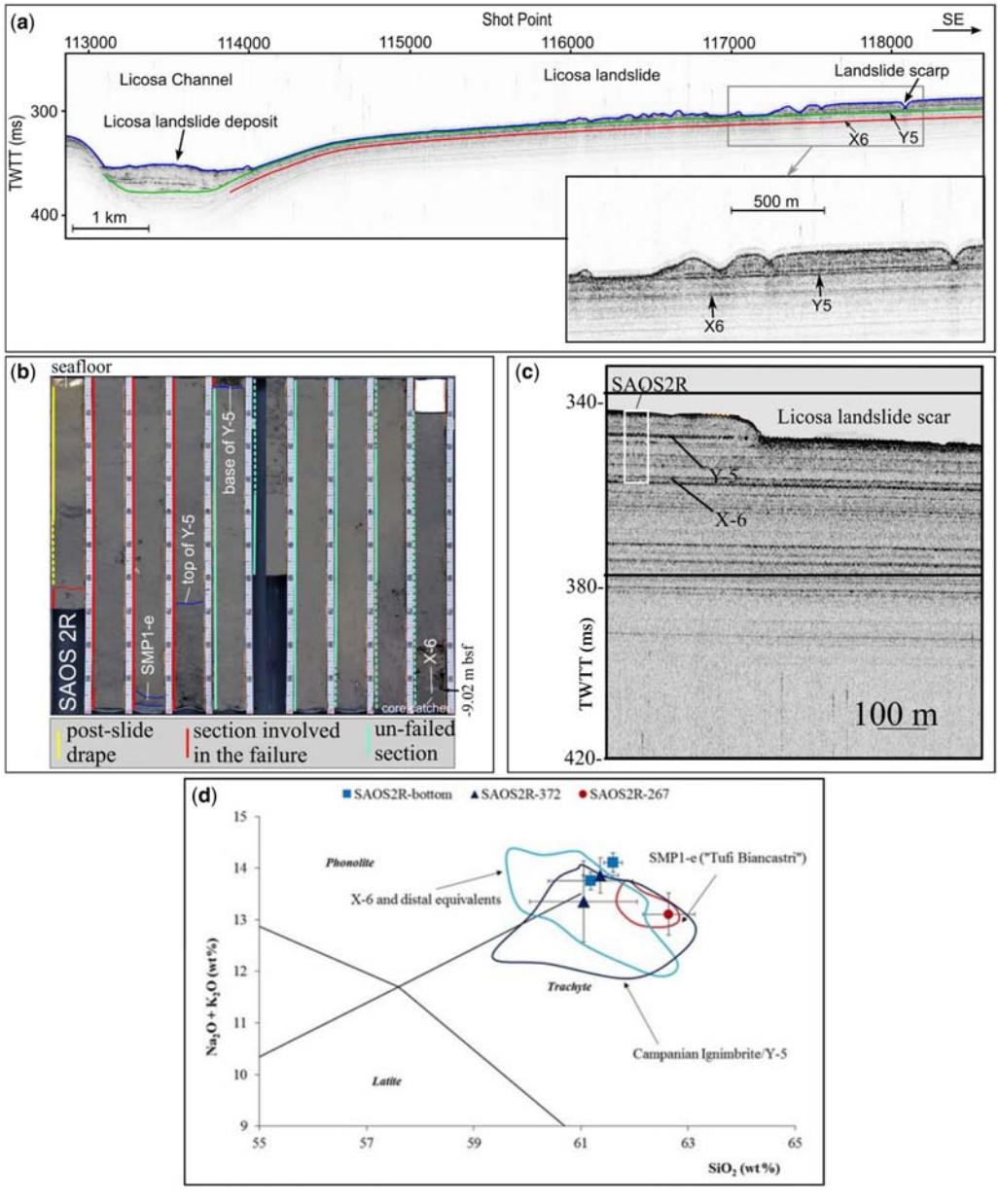

Fig. 7. (**a**) CHIRP profile 8 across the Licosa landslide highlights the presence of three prominent reflections, two of which are tied to tephra layers: tephra X-6 (109 ka), in red, and the Campanian Ignimbrite tephra Y-5 (39 ka), in green. Vertical exaggeration is ×18. Location of the profile is shown in Figure 3. (**b**) The core SAOS-2R photograph depicts the 9.02 m-thick sediment record laterally to the landslide scar (core location in Fig. 1b); dashed lines mark the coarse-grained horizons; the blue lines bound the top and the bottom of Y-5 tephra. (**c**) CHIRP-Sonar section showing the in-scar and out-of-scar seismic stratigraphy, the lateral continuity of the seismic horizons, and the core SAOS-2R site; (**d**) Classification of the SAOS2R tephras according to the TAS diagram (Le Maitre 2005). The composition of tephras is reported as the average with error bars representing 1 standard deviation. The average compositional fields of their proximal and distal counterparts are reported for comparison. Dataset from: Di Vito *et al.* (2008), Insinga *et al.* (2014) and references therein, Tomlinson *et al.* (2012) and Albert *et al.* (2015) and references therein.

Table 1. *Averages and standard deviations (σ) of the major element composition of the SAOS2R tephras*

Tephra	SAO2R-bottom (X-6)				SAOS2R-372 (Y-5)				SAOS2R-267 (SMP1-e)	
	$n = 4$	σ	$n = 12$	σ	$n = 22$	σ	$n = 21$	σ	$n = 12$	σ
SiO_2	61.60	0.17	61.18	0.79	61.05	1.10	61.37	0.33	62.64	0.48
TiO_2	0.35	0.22	0.47	0.19	0.42	0.26	0.42	0.16	0.35	0.15
Al_2O_3	18.40	0.05	18.50	0.31	18.57	0.52	18.87	0.31	18.21	0.18
FeO_{tot}	3.06	0.13	3.22	0.34	3.27	0.86	3.05	0.27	2.88	0.22
MnO	0.42	0.39	0.25	0.14	0.22	0.14	0.22	0.13	0.07	0.09
MgO	0.34	0.07	0.49	0.14	0.61	0.33	0.33	0.09	0.43	0.10
CaO	1.69	0.10	2.00	0.22	2.36	0.65	1.77	0.11	2.23	0.27
Na_2O	7.18	0.06	5.32	0.83	4.07	0.96	6.18	0.40	4.43	0.30
K_2O	6.93	0.13	8.43	0.77	9.28	1.12	7.68	0.19	8.68	0.15
P_2O_3	0.04	0.07	0.14	0.12	0.15	0.16	0.11	0.13	0.09	0.10
Original total	94.09	1.26	93.59	1.89	97.09	1.24	97.11	0.87	95.68	1.16
Alk	14.11	0.19	13.75	0.17	13.35	0.79	13.86	0.34	13.11	0.41
K_2O/Na_2O	0.97	0.01	1.64	0.38	2.56	0.75	1.25	0.10	1.97	0.12

All analyses were recalculated water-free to 100%. The original totals are also reported.
n, number of analysed points; alk = $Na_2O + K_2O$.

Discussion

Stratigraphy and chronostratigraphic constraints

The acoustic basement is correlated to the hard-rock substratum composed of the Cilento Group and Monte Sacro formations outcropping on the Cilento promontory, unconformably overlying the siliciclastic and calciclastic succession, pertaining to the Nord-Calabrese (Middle Eocene–Burdigalian) and Parasicilide units (Lower Jurassic–Burdigalian?). These formations form the internal and the wedge-top nappes of the Southern Apennines chain (Vitale *et al.* 2011) emplaced since the Burdigalian (Bonardi *et al.* 2009).

The lithology of Unit 1, the deepest sedimentary unit resting on the hard-rock substratum, is not deducible by any direct investigation and is therefore highly speculative. We interpret it as a succession made of siliciclastic and bioclastic sands and pelites based on similarities with analogous features in present-day settings (Chiocci & Orlando 2004; Mongardi *et al.* 2004).

Correlation to the Milena and Margherita wells located in the Gulf of Salerno at a distance of about 25 km from the study area suggests that Unit 2 is made of clays and marly clays with intercalations of fine-grained sands (Sacchi *et al.* 1994) and possibly ash layers towards the top of the succession. The uppermost succession of Unit 2 has been correlated with Marine Isotopic Stage (MIS) 8 (*c.* 300–245 ka BP), which was characterized by regression and a subsequent lowstand phase of sea level (Ferraro *et al.* 1997).

Units 3 and 4 correlate with MIS 7 (243–191 ka BP) and MIS 6 (191–130 ka BP), respectively, and consist of pelites with intercalations of volcanic and bioclastic sand and tephra layers (Trincardi *et al.* 2003; Aucelli *et al.* 2012; Budillon *et al.* 2014; Iorio *et al.* 2014).

Unit 5 is correlated to MIS 5–MIS 1, encompassing the regression and subsequent lowstand phase of sea level during MIS 4 and MIS 2.

Tephra SAOS2R-bottom can be correlated with the main marker tephra X-6 (108.9 ± 1.8 ka: Iorio *et al.* 2014) which occurs in terrestrial and marine archives of the Central Mediterranean area (Insinga *et al.* 2014 and references therein), and is characterized by an homogenous silica value (61–62 wt%) and distinctive K_2O/Na_2O value ranging from ≤1 to ≥2.

Tephra SAOS2R-372 can be considered as an equivalent of the main marker tephra Y-5 sourced by the Campanian Ignimbrite eruptive event that occurred at Campi Flegrei at 39.85 ± 0.14 ka (Giaccio *et al.* 2017). The proposed correlation is strongly supported by the regular occurrence in the three analysed samples of two main populations characterized by K_2O/Na_2O average values at *c.* 1.25 and *c.* 2.5 (Fig. 7; Table 1) which are typically detected in fall and pyroclastic flow proximal deposits, and ascribable to different degrees of magma evolution (Fedele *et al.* 2008; Tomlinson *et al.* 2012).

According to chemistry (silica values at 62–63 wt% with $K_2O/Na_2O \geq 2$) and stratigraphic position (above the Campanian Ignimbrite tephra), tephra SAOS2R-267 can be correlated with the Phlegrean 'Tufi Biancastri' deposits, which include the eruptive products emplaced between the Campanian

Ignimbrite and the Neapolitan Yellow Tuff (*c.* 15 ka: Deino *et al.* 2004) events. In terms of major element composition, the analysed tephra matches well with the SMP1-e deposits (Fig. 7) cropping out at the Sorrentina Peninsula and dated as 30.72–29.39 cal ka (Di Vito *et al.* 2008; Albert *et al.* 2015).

Tephras X-6 and Y-5 can be tied to two prominent reflections in the sub-bottom profiler data (Fig. 7a, c). The Y-5 reflection can be traced continuously from below the depocentre of the sedimentary wedge landwards of the landslide to the headwall and below the relict blocks, and it merges with the seafloor reflection in the translational area.

Tephra Y-5 is an important chronostratigraphic horizon and it has been used to calculate the sedimentation rate in the area during the last glacial MIS 3–MIS 2 (Lisiecki & Raymo 2005) sea-level lowering and lowstand, which account for the building of the uppermost sedimentary wedge. The maximum thickness of the wedge is 0.0837 s TWTT in the area NE of the landslide scar. With a minimum and maximum constant velocity of 1500 and 1700 m s^{-1}, the maximum thickness results are between 62.72 and 71.15 m, respectively (Fig. 3a). The sedimentation rate between the deposition of Y-5 and the slide event was found to be between 2.24 and 2.54 mm a^{-1}. In calculating the sedimentation rate, we did not consider the sedimentation over the last 11 ka which is represented by 65 cm of Holocene deposits. The isopach map of the post-Campanian Ignimbrite sedimentary wedge until the onset of the Holocene is illustrated in Figure 3a, where lines identify the thickness in metres, calculated assuming a constant velocity of 1700 m s^{-1}.

As far as the age of the Licosa landslide is concerned, for the purpose of this analysis, it is considered over the time period ranging from 14 to 11 ka, following the conclusions of Trincardi *et al.* (2003) and Iorio *et al.* (2014), respectively.

The fluid-emission phase responsible for the pockmarks below the Licosa landslide appears to be confined to Unit 2, between 300 and 245 ka (MIS 8). Being the layer-bound subvertical extensional fault system dissecting the area of the buried pockmarks sealed by the erosional surface separating Unit 4 and Unit 5, their activity appears to have lasted longer, throughout the time of deposition of units 2, 3 and 4, and before the Unit 4 top unconformity: therefore until *c.* 150 ka. This age of the pockmarks formation and layer-bound fault activity can be correlated to the Mid-Pleistocene tectonic extension phase related to the opening of the Southern Tyrrhenian Basin (Caiazzo *et al.* 2006).

Geological constraints for slope instability

In the following subsections, we address the geological constraints that guide the slope-stability analysis.

Erosion of the base of the slope. The Licosa landslide occurs upslope from the Licosa submarine channel in which the mass-transport deposit (MTD) of the landslide has accumulated. Even if basal removal of support is not a process commonly considered as a trigger of submarine landslides (e.g. see reviews by Canals *et al.* 2004; Masson *et al.* 2006; Lee 2009; Talling *et al.* 2014; Shanmungam 2015), the undercutting of the slope by turbidity currents or contour currents may result in an increase of the shear stress and consequent instability of the sediments above (Hühnerbach *et al.* 2004; Lee *et al.* 2007).

The Licosa Channel at the base of the failed slope is a small-sized (maximum width less than 1 km) channel emplaced along a major subvertical fault system. We cannot identify any evidence in the seismic reflection data for basal erosion of the slope.

However, an erosional surface is located on the northern side of the channel, stratigraphically deeper than the Licosa landslide scarp (white dotted line in Fig. 4). This erosional surface is identified as the headwall of the landslide that lies deeper in the Licosa channel floor and which produced the lower, smaller volume, MTD. In this case, the slope failure appears to have originated from the channel sidewall, and basal undercutting could be considered as an initiating triggering mechanism.

Sea-level rise. Whether sea-level rise could play an important role in landslide occurrence is still an open debate (Smith *et al.* 2013; Talling *et al.* 2014). Smith *et al.* (2013) identified a rapid sea-level rise as a possible cause of slope instability, taking as an example the Storegga landslide on the Norwegian margin that occurred during the early Holocene sea-level rise. Sea-level rise could have influenced the slope stability both by increasing the pore pressure of slope sediments and by inducing seismic activity through the reactivation of faults due to the flexure of continental shelves under the increased weight of the water column.

Trincardi *et al.* (2003) suggested that rapid loading and drowning of unconsolidated sediments played a role in the initiation of the Licosa landslide. The hypothesis is supported by the coincidence of the age of the landslide with Melt Water Pulse 1A (Clark *et al.* 1996), when sea level rose by about 20 m in a time span of 500 years. The consequent increase in hydrostatic pressure propagating in the pore space of an underconsolidated sedimentary sequence would have induced a decrease in the effective stress, thus reducing the stability of the slope.

Urlaub *et al.* (2013) took into consideration 68 different landslides from open continental slope settings and which involved a total volume of at least 1 km^3. The statistical analysis that was carried out did not highlight any evidence of significant

correlation between sea-level rise and landslide frequency. Furthermore, Talling *et al.* (2014) argued that an increase in the height of the water column alone cannot determine an increase in the excess pore pressure and, hence, a decrease in effective stress with respect to a normal consolidation state. This applies, however, only in the case of high permeability. In a low-permeability environment, a rapid increase in the load of the water column could result in a pressure pulse that would cause excess pore pressure with a low rate of dissipation. Such a transient pressure pulse could decrease the effective stress significantly; particularly in shallow sediments where the difference between hydrostatic and lithostatic load is small.

The lowstand sedimentary wedge where the Licosa landslide occurred is expected to be composed of sediments with a grain size varying from sands in the inner and upper part of the wedge, to muds in the lower and outer part (e.g. Martorelli *et al.* 2014). Furthermore, the occurrence of tephras provides high-permeability layers intercalated with low-permeability muds of the outer wedge. Therefore, rapidly rising sea level may have played a role in reducing the strength of the sediments in the shallow, lower slope sediments of the wedge.

Earthquake shaking. Earthquakes are considered by far the most common triggering mechanism of submarine landslides (e.g. Talling *et al.* 2014). The cyclic loading produced by earthquakes increases the shear stress on the sediment column. In low-permeability sediments, it induces accumulation of excess pore pressure and a consequent decrease in the shear strength. In high-permeability (sandy) sediments, earthquake shaking may cause liquefaction and loss of shear strength (Locat & Lee 2005). In addition, strain softening effects may decrease the sediment shear strength (e.g. Lee *et al.* 2007). On the other hand, if cyclic loading does not induce failure, the overall effect on the sediment may be that of strain strengthening; thus explaining the small size and low occurrence of submarine landslides in tectonically active areas with a high frequency of occurrence of earthquakes, such as the Oregon margin (McAdoo *et al.* 2000). Well-documented cases of correlation between seismicity and submarine slope failure are still rare. The 1929 Grand Banks slope failure is probably the best-documented case, where a magnitude 7.2 earthquake initiated a sequence of slope failures evolving to turbitidy currents that broke, in a sequence, several submarine telecommunication cables, and generated an important tsunami on the adjacent Nova Scotia coast (e.g. Piper *et al.* 1999; Løvholt *et al.* 2018; Schulten *et al.* 2018). Similarly, convincing correlation between the historical 1663 and 1988 earthquakes and submarine slope failure has been provided in the upper Saguenay Fjord in Quebec, Canada (Urgeles *et al.* 2002; Locat *et al.* 2003). The occurrence of earthquake-induced landslides depends not only on the earthquake magnitude and location but also on the sedimentation history of the area. As an example, Wilhelm *et al.* (2016) pointed out how most of the landslides in Hardangerfjorden occurred during high sedimentation rate intervals.

At present, the Campanian margin of the Tyrrhenian Sea seems to be affected by two types of earthquakes:

- Very deep epicentres (as deep as 500 km) are located below the Southern Tyrrhenian Basin along a NE–SW-striking and NW-dipping Benioff plane. Focal mechanisms are consistent with downdip subduction of the Ionian crust below the Calabrian crustal block extending along the continental margin a few tens of kilometres seawards of the Licosa landslide location (Vannucci *et al.* 2004, fig. 11).
- Shallow (10–12 km) epicentres occur onshore in a narrow belt corresponding to the highest relief of the Southern Apennine chain and include the largest magnitude events on the Italian peninsula. Focal mechanisms show extensional geometry throughout the chain, induced by the Tyrrhenian Sea back-arc extension. This belt is located about 60–70 km inland with respect to the Licosa submarine landslide. No significant seismicity is presently outlined onshore, on the Cilento promontory (see the seismic hazard map of Italy published by the Italian Civil Defence Department: http://www.protezionecivile.gov.it/jcms/en/classificazione.wp). Offshore, the catalogue of the International Seismologic Centre (http://www.isc.ac.uk) reports several events with magnitude >3, including one M5 event, in the last 100 years (Storchak *et al.* 2013).

However, the region surrounding the Licosa landslide is affected by at least one important tectonic discontinuity, the Licosa Channel Fault System (Fig. 8), causing vertical offset of several hundreds of metres in the hard-rock substratum, significant tilting in the sedimentary formations, erosional surfaces and offsetting the most recent sedimentary sequences, including the youngest Unit 5 (Fig. 2).

According to our interpretation, the Licosa Channel Fault is a structure with significant evidence of recent, possibly present, activity. Movements along this fault may cause ground accelerations that should be considered as potential triggers of submarine slope instability in the area.

Ash layers. Ash layers have been identified as glide planes for submarine landslides (Harders *et al.* 2010; Sassa *et al.* 2012; Wiemer *et al.* 2015; Wiemer & Kopf 2015). However, their role in generating

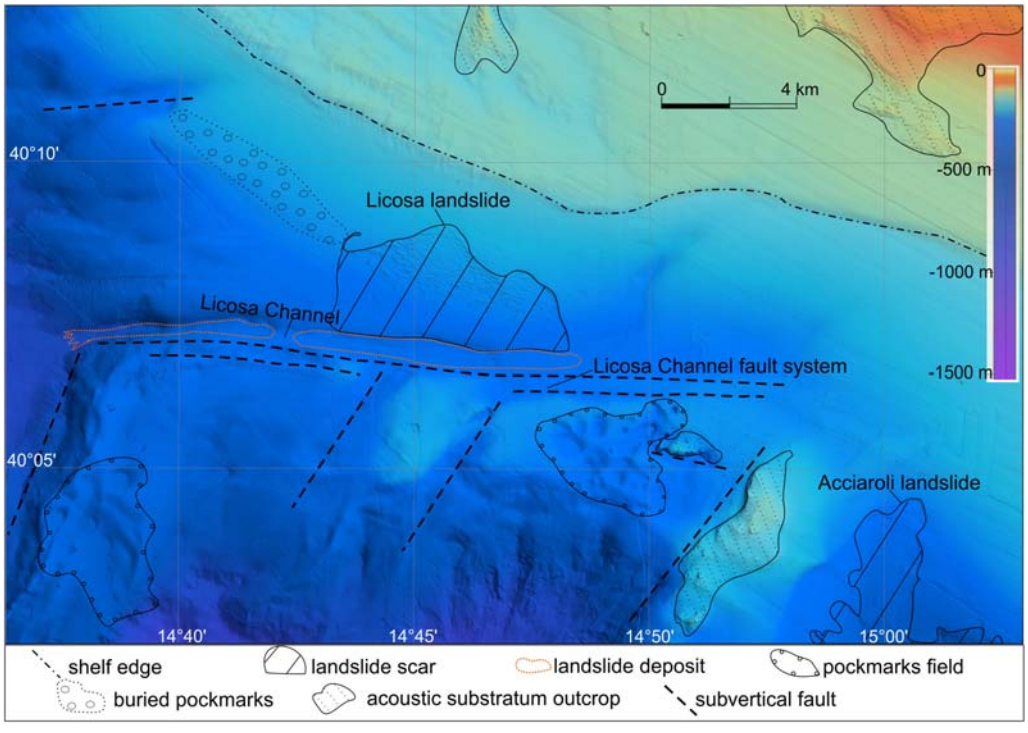

Fig. 8. Sketch of the main structural lineaments resulting from combining the DTM analysis with the interpretation of multichannel seismic sections. The east–west and NE–SW fault trends identified in the area are consistent with the definition of the fourth, active deformation event characterized by an extensional regime with a NE–SW-trending principal stress σ_3 (Caiazzo *et al.* 2006).

instability is still unclear. Two different mechanisms that could induce weakness have been proposed. The first approach (Harders *et al.* 2010; Wiemer *et al.* 2015) is based on the fact that the soil skeleton of tephra layers is formed by highly crushable glass particles disposed in a relatively loose state. When a certain level of shear stress, most probably applied by an earthquake, acts on the tephra layer, it may cause rearrangement and even crushing of the particles with consequent compaction and volumetric contraction. This reduction in pore space generates excess porewater pressures similar to a mechanism of liquefaction, with consequent reduction in the effective stress and thus in shear strength. The volcanic ash layer can, therefore, become a weak detachment surface. In tephra layers, this process can be considered a mechanism of liquefaction and is enhanced by the large difference in hydraulic conductivity between the ash layer and the sandwiching sediments that do not allow porewater drainage. Wiemer & Kopf (2015) investigated an alternative mechanism that could transform a volcanic ash layer to a weak layer due to changes in the intrinsic properties only. Fresh ash layers are normally characterized by a high shear strength due to particle roughness and angularity. If alteration of volcanic glass shards forming the layer occurs, it results in a significant decrease in the shear strength due to the increase in content of authigenic clay minerals (primarily smectite). Therefore, a highly altered ash layer could potentially play a role in slope failure by acting as a weak layer within a sedimentary sequence. Data from drill holes suggest that in order to achieve a level of alteration high enough to create instability, long periods and high burial depths are necessary. In the Licosa landslide area, ash-layer alteration is not observed in the samples, and can be excluded due to the shallow depth and young age of tephra Y-5.

Liquefaction of tephra layers in response to earthquake shaking should be considered in slope-stability analysis given the recurrence of such layers derived from the volcanic eruption history within the Campanian Province in the Late Pleistocene–Holocene.

Subsurface fluid migration. Buried, or relict, pockmarks are common in the stratigraphic record and identify periods of fluid, generally methane gas,

emissions from the seabed (e.g. Judd & Hovland 2007). The frequent association of pockmarks and fluid/gas-emission structures with submarine landslides in the Mediterranean suggests that fluid flow is a major factor controlling the initiation of slope failure (Urgeles & Camerlenghi 2013). The buried pockmarks imaged in seismic profile LIC 06 (Fig. 5) indicate gas emissions NW of the Licosa landslide that extend partly stratigraphically below the detachment zone of the landslide. The buried pockmarks are associated with a set of layer-bound, near-vertical normal faults that are likely to represent a polygonal fault system. Pockmark formation is probably related to the onset of Campanian volcanic activity and excludes any link with the emplacement of the Licosa landslide. Recent fluid emissions are suggested by pockmarks SE of the Licosa landslide (Fig. 6a) which retain a morphological imprint on the seafloor. However, no evidence of fluid emission is present at the seafloor or in the shallow subsurface of the Licosa landslide area. We conclude that overpressure induced by upwards gas migration does not alter the pore pressure regime and, thus, did not play a role in the sediment failure that generated the Licosa landslide.

High sedimentation rate and lateral flow. A key factor for slope instability is excess pore pressure, and consequent reduction in shear strength, that may be induced by the rapid accumulation of low-permeability sediments. Jones (1968) considered high sedimentation rate as the main factor in generating abnormally high fluid pressures and therefore slope instability in the northern Gulf of Mexico. The development of excess pore pressure by sedimentation alone depends on both sedimentation rate and permeability. A sedimentation rate in excess of 1 mm a^{-1} is considered capable of generating overpressure in fine-grained (clay-rich) sediments (Rubey & Hubbert 1959; Fertl 1976). It has been demonstrated that the excess pore pressure generated by rapid loading may affect slope stability by also inducing laterally focused fluid flow along a high-permeability layer towards the lower slope. This lateral flow moves fluids away from the sediment depocentre towards an area where lower lithostatic load may amplify the state of underconsolidation in the sedimentary succession (Dugan & Flemings 2002). Below the New Jersey continental slope, a layer of permeable sandy silt of Miocene age was asymmetrically buried by Pleistocene sedimentation. The deposition of low-permeability silt and clay has continued for 1 myr with a high sedimentation rate (>1 mm a^{-1}) generating excess pressure. The highest overpressure is produced in the landwards zone, where the sedimentation rate was highest. However, instability occurs seawards, in an area of lower sedimentation rate at the base of the continental slope. A 2D model suggests that a lateral flow of overpressured porewater along the Miocene permeable layer is capable of increasing the overpressure at the base of the slope, reducing slope stability (Dugan & Flemings 2002). Flemings *et al.* (2002) focused on a similar situation in the Gulf of Mexico, where high-sedimentation, low-permeability mudstones overlay a dipping permeable sandstone layer. In this case, the lateral flow along the sandstone explains an increase in pressure seawards generating the instability. Both studies highlight how local sedimentation rate and flow focusing are the two main compelling mechanisms in controlling the overpressure and slope stability.

Even if deposition times and thickness of the sediments are smaller than in the New Jersey margin and Gulf of Mexico cases, the stratal geometry of the Licosa landslide area deserves an attempt to evaluate similar mechanisms and their influence on stability conditions. The sedimentary depocentre of the lowstand sedimentary wedge is located upslope of the landslide, and the average sedimentation rate in the last 39 kyr has varied between 2.24 and 2.54 mm a^{-1} – well above the threshold considered for the development of overpressure in fine-grained sediments. The nature of the sedimentary succession in the wedge is not known. However, these sedimentary wedges are typically composed of an upper, prograding coarse-grained unit overlying and passing laterally to a fine-grained unit that constitutes the bulk of the wedge. The distal portion of the wedge, where the Licosa landslide occurred, is composed of an ash-layer-bearing sandy-silty clay with a sedimentation rate of about one order of magnitude lower and values of permeability, and hence consolidation coefficient, higher than those typical of purely pelitic sequences. The seawards-dipping, conformable ash layer Y-5 connects the depocentre of the wedge to the distal lower slope. Such stratigraphy could have generated a situation where overpressured porewater flow along the Y-5 ash layer increased the excess pore pressure in the distal lower slope. Therefore, the influence of excess pore pressure due to sedimentation could have been a factor that increased the initial pore pressure level.

Conclusions

The analysis of the regional geological structure in the area surrounding the Licosa landslide has revealed that a number of processes, not considered before, are likely to contribute to weakening the slope and favour failure under the action of an external trigger:

- The detachment surface of the Licosa landslides coincides with a marker bed composed of the tephra layer Y-5 (*c.* 39 ka) correlated to the

Campanian Ignimbrite deposit generated by Phlegrean Fields super-eruption and caldera collapse. This marker bed allows the calculation of an average sedimentation rate over the last 39 kyr of between 2.24 and 2.54 mm a^{-1} in the depocentre of the wedge.

- Ash layer Y-5 appears as the potential candidate for the weak layer given the known mechanical behaviour of such a lithology under cyclic loading. Volcanic ash alteration is not demonstrated in core data and cannot be considered as a mechanism for shear strength decrease in this case.
- The calculated sedimentation rate in the depocentre of the sedimentary wedge is capable of generating excess porewater pressure in the layers of the lowstand sedimentary wedge with a higher clay fraction. In particular, lateral flow transfer from the overpressured sedimentary wedge depocentre to the outer slope via the high-permeability conduits of the ash layer should be considered as a mechanism for decreasing the effective stress in the Licosa landslide area.
- Rapid sea-level rise, previously invoked as a contributor of slope instability given the coincidence of the age of the landside with Meltwater Pulse 1A, may have contributed to generating an excess pore pressure if the sediment permeability is sufficiently low.
- Below the Licosa landslide MTD traced into the Licosa Channel, where it attains a maximum thickness of 25 m and a lateral extent of 600 m, there is another, older MTD with a maximum thickness of about 17 m and a lateral extent of 220 m. This older MTD originated from the failure of the northern slope of the channel as a prominent buried erosional scar bearing a clear morphological expression at the seafloor. Therefore, basal erosion of the slope in the Licosa Channel is unlikely to have affected the Licosa landslide that originated outside the channel, while such mechanism is likely to have generated the deeper MTD.
- Despite the recurrence of subsurface fluid-migration structures identified in the area, buried pockmarks below the landslide appear to be too old to have influenced the slope stability of the area. Other evidence of shallow gas/fluid migration is located outside the landslide area and cannot be identified as potential contributors to slope instability.
- Earthquake shaking is the most plausible external trigger of the slide. Even if the area does not show relevant historical seismicity onshore, induced by the proximity of the Southern Apennine shallow epicentre belt (Tyrrhenian extension), the occurrence offshore of earthquakes up to magnitude 5 in the last 100 years, and the presence of a large tectonic displacement along the Licosa Channel, allow speculation that the presence of an active fault has the potential to be responsible for the ultimate triggering of slope instability in the area. This prominent fault, not recognized before in the scientific literature, is likely to be the product of the current southern Tyrrhenian tectonic extension trending NE–SW, active since the Middle Pleistocene. The very deep epicentres of the southern Tyrrhenian (plate subduction) are less likely to produce the significant ground shaking that would cause slope instability.

Acknowledgments The captain and crew of the research vessels OGS *Explora* and *Urania* are warmly acknowledged for their constructive and cooperative attitude during the data-acquisition phases. We thank HIS Global Inc. for providing an academic educational licence for KingdomSuite, and Roberto de' Gennaro for his assistance during microprobe acquisition. P. Tommasi, A. Avalle, and A. Pagliaroli improved the data discussion in relation to geotechnical issues. We acknowledge the constructive reviews by G. Wiemer, an anonymous reviewer and editor D.C. Mosher.

Funding Ministero dell'Istruzione, dell'Università e della Ricerca (IT) and the National Research Program Flagship Project RITMARE – The Italian Research for the Sea, coordinated by the Italian National Research Council awarded grants to A. Camerlenghi and F. Budillon.

References

Albert, P.G., Hardiman, M. *et al.* 2015. Revisiting the Y-3 tephrostratigraphic marker: a new diagnostic glass geochemistry, age estimate, and details on its climatostratigraphical context. *Quaternary Science Reviews*, **118**, 105–121.

Aucelli, P.P., Amato, V. *et al.* 2012. Evolution of the Sele River coastal plain (southern Italy) during the Late Quaternary by inland and offshore stratigraphical analyses. *Rendiconti Lincei*, **23**, 81–102.

Bellonia, A., Budillon, F., Trincardi, F., Insinga, D., Iorio, M., Asioli, A. & Marsella, E. 2008. Licosa and Acciaroli submarine slides, Eastern Tyrrhenian margin: characterisation of a possible common weak layer. *Rendiconti Online Società Geologica Italiana*, **3**, 83–84.

Bonardi, G., Ciarcia, S., Di Nocera, S., Matano, F., Sgrosso, I. & Torre, M. 2009. Catalogo delle principali unità cinematiche dell'Appennino meridionale. *Italian Journal of Geosciences*, **128**, 47–60.

Budillon, F., Conforti, A., Tonielli, R., De Falco, G., Di Martino, G., Innangi, S. & Marsella, E. 2011. The Bulgheria canyon-fan: a small scale, proximal system in the eastern Tyrrhenian Sea (Italy). *Marine Geophysical Researches*, **32**, 83–97.

Budillon, F., Cesarano, M., Conforti, A., Pappone, G., Di Martino, G. & Pelosi, N. 2014. Recurrent superficial sediment failure and deep gravitational deformation in a Pleistocene slope marine succession: the Poseidonia

Slide (Salerno Bay, Tyrrhenian Sea). *In*: Krastel, S., Behrmann, J.-H. *et al.* (eds) *Submarine Mass Movements and Their Consequences*. Advances in Natural and Technological Hazards Research, **37**. Springer International, Cham, Switzerland, 273–283, https://doi.org/10.1007/978-3-319-00972-8_24

Caiazzo, C., Ascione, A. & Cinque, A. 2006. Late Tertiary–Quaternary tectonics of the Southern Apennines (Italy): new evidences from the Tyrrhenian slope. *Tectonophysics*, **421**, 23–51.

Canals, M., Lastras, G. *et al.* 2004. Slope failure dynamics and impacts from seafloor and shallow sub-seafloor geophysical data: case studies from the COSTA project. *Marine Geology*, **213**, 9–72.

Chiocci, F.L. & Orlando, L. 2004. Terrazzi deposizionali sommersi nel settore meridionale del Golfo di S. Eufemia (Calabria). *Memorie Descrittive della Carta Geologica d'Italia*, **58**, 75–80.

Clark, P.U., Alley, R.B., Keigwin, L.D., Licciardi, J.M., Johnsen, S.J. & Wang, H. 1996. Origin of the first global meltwater pulse following the last glacial maximum. *Paleoceanography*, **11**, 563–577.

D'Argenio, B., Aiello, G. *et al.* 2004. Digital elevation model of the Naples Bay and adjacent areas, Eastern Tyrrhenian Sea. *In*: Pasquarè, G., Venturini, C. & Groppelli, G. (eds) *Mapping Geology in Italy*. Agenzia per la Protezione dell'Ambiente e per i Servizi Tecnici (APAT), Firenze, Italy, 21–28.

Deino, A.L., Orsi, G., de Vita, S. & Piochi, M. 2004. The age of the Neapolitan Yellow Tuff caldera – forming eruption (Campi Flegrei Caldera – Italy) assessed by $^{40}Ar/^{39}Ar$ dating method. *Journal of Volcanology and Geothermal Research*, **133**, 157–170.

Di Vito, M., Sulpizio, R., Zanchetta, R. & D'Orazio, M. 2008. The late Pleistocene pyroclastic deposits of the Campanian Plain: new insights on the explosive activity of Neapolitan volcanoes. *Journal of Volcanology and Geothermal Research*, **177**, 19–48.

Dugan, B. & Flemings, P.B. 2002. Fluid flow and stability of the US continental slope offshore New Jersey from the Pleistocene to the present. *Geofluids*, **2**, 137–146.

Faccenna, C., Becker, T.W., Lucente, F.P., Jolivet, L. & Rossetti, F. 2001. History of subduction and back arc extension in the Central Mediterranean. *Geophysical Journal International*, **145**, 809–820.

Fedele, L., Scarpati, C., Lanphere, M., Melluso, L., Morra, V., Perrotta, A. & Ricci, G. 2008. The Breccia Museo formation, Campi Flegrei, southern Italy: geochronology, chemostratigraphy and relationship with the Campanian Ignimbrite eruption. *Bulletin of Volcanology*, **70**, 1189–1219.

Ferraro, L., Pescatore, T., Russo, B., Senatore, M.R., Vecchione, C., Coppa, M.G. & Di Tuoro, A. 1997. Studi di geologia marina del margine tirrenico; la piattaforma continentale tra Punta Licosa e Capo Palinuro (Tirreno meridionale). *Bollettino della Società geologica italiana*, **116**, 473–485.

Fertl, W.H. 1976. *Abnormal Formation Pressures. Implications to Exploration, Drilling, and Production of Oil and Gas Resources*. Developments in Petroleum Science, **2**. Elsevier, Amsterdam.

Flemings, P.B., Stump, B.B., Finkbeiner, T. & Zoback, M. 2002. Flow focusing in overpressured sandstones: theory, observations, and applications. *American Journal of Science*, **302**, 827–855.

Giaccio, B., Hajdas, I., Isaia, R., Deino, A. & Nomade, N. 2017. High-precision ^{14}C and $^{40}Ar/^{39}Ar$ dating of the Campanian Ignimbrite (Y-5) reconciles the time-scales of climatic-cultural processes at 40 ka. *Scientific Reports*, **7**, 45940, https://doi.org/10.1038/srep45940

Insinga, D.D., Tamburrino, S. *et al.* 2014. Tephrochronology of the astronomically-tuned KC01B deep-sea core, Ionian Basin: insights into the explosive activity of the Central Mediterranean area between 16 ka and 200 ka. *Quaternary Science Reviews*, **85**, 63–84.

Hamilton, E.L. 1978. Sound velocity–density relations in sea-floor sediments and rocks. *Journal of the Acoustical Society of America*, **63**, 366–377.

Harders, R., Kutterolf, S., Hensen, C., Moerz, T. & Brueckmann, W. 2010. Tephra layers: a controlling factor on submarine translational sliding? *Geochemistry, Geophysics, Geosystems*, **11**, Q05S23.

Hühnerbach, V., Masson, D.G. & partners of the COSTA-Project 2004. Landslides in the North Atlantic and its adjacent seas: an analysis of their morphology, setting and behaviour. *Marine Geology*, **213**, 343–362.

Iorio, M., Liddicoat, J. *et al.* 2014. Combined palaeomagnetic secular variation and petrophysical records to time-constrain geological and hazardous events: an example from the eastern Tyrrhenian Sea over the last 120 ka. *Global and Planetary Change*, **113**, 91–109.

Jones, P.H. 1968. *Hydrology of Neogene deposits in the northern Gulf of Mexico basin*. PhD thesis, Louisiana State University.

Judd, A.G. & Hovland, M. 2007. *Seabed Fluid Flow: The Impact on Geology, Biology and the Marine Environment*. University Press, Cambridge.

Lee, H.J. 2009. Timing of occurrence of large submarine landslides on the Atlantic Ocean margin. *Marine Geology*, **264**, 53–64.

Lee, H.J., Locat, J. *et al.* 2007. Submarine mass movements on continental margins. *In*: Nittrouer, C.A., Austin, J.A., Field, M.E., Kravitz, J.H., Syvitski, J.P.M. & Wiberg, P.L. (eds) *Continental Margin Sedimentation: from Sediment Transport to Sequence Stratigraphy*. International Association of Sedimentologists, Special Publications, **37**, 213–274.

Le Maitre, R.W. 2005. *Igneous Rocks. A Classification and Glossary of Terms. Recommendations of the International Union of Geological Sciences Subcommission on the Systematics of Igneous Rocks*. Cambridge University Press, Cambridge.

Lisiecki, L.E. & Raymo, M.E. 2005. A Pliocene-Pleistocene stack of 57 globally distributed benthic $\delta^{18}O$ records. *Paleoceanography*, **20**, PA1003, https://doi.org/10.1029/2004PA001071

Locat, J. & Lee, H.J. 2005. Subaqueous debris flows. *In*: Jakob, M. & Hungr, O. (eds) *Debris-Flow Hazards and Related Phenomena*. Springer, Berlin, 203–245.

Locat, J., Martin, F., Levesque, C., Locat, P., Leroueil, S., Konrad, J.-M., Urgeles, R., Canals, M. & Duchesne, M.J. 2003. Submarine mass movements in the Upper Saguenay Fjord, (Québec, Canada), triggered by the 1663 earthquake. *In*: Locat, J. & Mienert, J. (eds) *Submarine Mass Movements and their Consequences*, Kluwer, 509–519.

Løvholt, F., Schulten, I., Mosher, D., Harbitz, C. & Krastel, S. 2018. Modelling the 1929 Grand Banks slump and landslide tsunami. *In*: Lintern, D.G. & Mosher, D.C. *et al.* (eds) *Subaqueous Mass Movements and their Consequences*, Geological Society, London, Special Publications, **477**, https://doi.org/10.1144/SP477.28

Magagnoli, M. 2017. A new coring method in deep water. *Marine Georesources and Geotechnology*, **35**, 496–503.

Malinverno, A. & Ryan, W.B. 1986. Extension in the Tyrrhenian Sea and shortening in the Apennines as result of arc migration driven by sinking of the lithosphere. *Tectonics*, **5**, 227–245.

Margaritelli, G., Vallefuoco, M. *et al.* 2016. Marine response to climate changes during the last five millennia in the central Mediterranean Sea. *Global and Planetary Change*, **142**, 53–72.

Martorelli, E., Falese, F. & Chiocci, F.L. 2014. Overview of the variability of Late Quaternary continental shelf deposits of the Italian peninsula. *In*: Chiocci, F.L. & Chivas, A.R. (eds) *Continental Shelves of the World: Their Evolution During the Last Glacio-Eustatic Cycle*. Geological Society, London, Memoirs, **41**, 171–186, https://doi.org/10.1144/M41.12

Masson, D.G., Harbitz, C.B., Wynn, R.B., Pedersen, G. & Løvholt, F. 2006. Submarine landslides: processes, triggers and hazard prediction. *Philosophical Transactions of the Royal Society of London A: Mathematical, Physical and Engineering Sciences*, **364**, 2009–2039.

Mattei, M., Cipollari, P., Cosentino, D., Argentieri, A., Rossetti, F., Speranza, F. & Di Bella, L. 2002. The Miocene tectono-sedimentary evolution of the southern Tyrrhenian Sea: stratigraphy, structural and palaeomagnetic data from the on-shore Amantea basin (Calabrian Arc, Italy). *Basin Research*, **14**, 147–168.

McAdoo, B.G., Pratson, L.F. & Orange, D.L. 2000. Submarine landslide geomorphology, US continental slope. *Marine Geology*, **169**, 103–136.

Milia, A. 2000. The Dohrn canyon: a response to the eustatic fall and tectonic uplift of the outer shelf along the eastern Tyrrhenian Sea margin, Italy. *Geo-Marine Letters*, **20**, 101–108.

Mongardi, S., Correggiari, A. & Trincardi, F. 2004. Terrazzi deposizionali sommersi al largo di Capo Suvero. *In*: Chiocci, F.L., D'Angelo, S. & Romagnoli, C. (eds) *Atlante dei terrazzi deposizionali sommersi lungo le coste italiane*. Memorie descrittive della Carta Geologica d'Italia, **58**, 63–74.

Pabst, S., Wörner, G., Civetta, L. & Tesoro, R. 2008. Magma chamber evolution prior to the Campanian Ignimbrite and Neapolitan Yellow Tuff eruptions (Campi Flegrei, Italy). *Bulletin of Volcanology*, **70**, 961–976.

Peccerillo, A. 2016. *Cenozoic Volcanism in the Tyrrhenian Sea Region*. Springer, Berlin.

Piper, D.J., Cochonat, P. & Morrison, M.L. 1999. The sequence of events around the epicentre of the 1929 Grand Banks earthquake: initiation of debris flows and turbidity current inferred from sidescan sonar. *Sedimentology*, **46**, 79–97.

Prada, M., Sallarès, V., Ranero, C.R., Vendrell, M.G., Grevemeyer, I., Zitellini, N. & Franco, R. 2014. Seismic structure of the Central Tyrrhenian basin: geophysical constraints on the nature of the main crustal domains. *Journal of Geophysical Research: Solid Earth*, **119**, 52–70.

Rubey, W.W. & Hubbert, M.K. 1959. Role of fluid pressure in mechanics of overthrust faulting: II. Overthrust belt in geosynclinal area of western Wyoming in light of fluid-pressure hypothesis. *Geological Society of America Bulletin*, **70**, 167–206.

Sacchi, M., Infuso, S. & Marsella, E. 1994. Late Pliocene-Early Pleistocene compressional tectonics in offshore campania (Eastern Tyrrhenian sea). *Bollettino di Geofisica Teorica ed Applicata*, **36**, 469–482.

Sassa, K., He, B. *et al.* 2012. A hypothesis of the Senoumi submarine megaslide in Suruga Bay in Japan – based on the undrained dynamic-loading ring shear tests and computer simulation. *Landslides*, **9**, 439–455.

Schulten, I., Mosher, D.C., Krastel, S., Piper, D.J.W. & Kienast, M. 2018. Surficial sediment failures due to the 1929 Grand Banks Earthquake, St Pierre Slope. *In*: Lintern, D.G. & Mosher, D.C. *et al.* (eds) *Subaqueous Mass Movements and their Consequences*, Geological Society, London, Special Publications, **477**, https://doi.org/10.1144/SP477.25

Shanmungam, G. 2015. The landslide problem. *Journal of Paleogeography*, **4**, 109–166.

Smith, D.E., Harrison, S. & Jordan, J.T. 2013. Sea level rise and submarine mass failures on open continental margins. *Quaternary Science Reviews*, **82**, 93–103.

Storchak, D.A., Di Giacomo, D., Bondár, I., Engdahl, E.R., Harris, J., Lee, W.H.K., Villaseñor, A. & Bormann, P. 2013. Public release of the ISC-GEM global instrumental earthquake catalogue (1900–2009). *Seismology Research Letters*, **84**, 810–815.

Talling, P.J., Clare, M.L., Urlaub, M., Pope, E., Hunt, J.E. & Watt, S.F. 2014. Large submarine landslides on continental slopes: geohazards, methane release, and climate change. *Oceanography*, **27**, 32–45.

Trincardi, F. & Field, M.E. 1992. Collapse and flow of lowstand shelf-margin deposits: an example from the eastern Tyrrhenian Sea, Italy. *Marine geology*, **105**, 77–94.

Trincardi, F., Cattaneo, A., Correggiari, A., Mongardi, S., Breda, A. & Asioli, A. 2003. Submarine slides during relative sea level rise: two examples from the eastern Tyrrhenian margin. *In*: Locat, J. & Mienert, J. (eds) *Submarine Mass Movements and Their Consequences*. Advances in Natural and Technological Hazards Research, **19**. Kluwer, Amsterdam, 469–478.

Tomlinson, E.L., Arienzo, I. *et al.* 2012. Geochemistry of the Phlegraean Fields (Italy) proximal sources for major Mediterranean tephras: implications for the dispersal of Plinian and co-ignimbritic components of explosive eruptions. *Geochimica et Cosmochimica Acta*, **93**, 102–128.

Urgeles, R. & Camerlenghi, A. 2013. Submarine landslides of the Mediterranean Sea: trigger mechanisms, dynamics, and frequency-magnitude distribution. *Journal of Geophysical Research: Earth Surface*, **118**, 2600–2618.

Urgeles, R., Locat, J., Lee, H.J. & Martin, F. 2002. The Saguenay Fjord, Quebec, Canada: integrating marine geotechnical and geophysical data for spatial seismic

slope stability and hazard assessment. *Marine Geology*, **185**, 319–340.

URLAUB, M., TALLING, P.J. & MASSON, D.G. 2013. Timing and frequency of large submarine landslides: implications for understanding triggers and future geohazard. *Quaternary Science Reviews*, **72**, 63–82.

VANNUCCI, G., PONDRELLI, S., ARGNANI, A., MORELLI, A., GASPERINI, P. & BOSCHI, E. 2004. An atlas of Mediterranean seismicity. *Annal of Geophysics*, **47**, 247–306.

VITALE, S., CIARCIA, S., MAZZOLI, S. & ZAGHLOUL, M.N. 2011. Tectonic evolution of the 'Liguride' accretionary wedge in the Cilento area, southern Italy: a record of early Apennine geodynamics. *Journal of Geodynamics*, **51**, 25–36.

WIEMER, G. & KOPF, A. 2015. Altered marine tephra deposits as potential slope failure planes? *Geo-Marine Letters*, **35**, 305–314.

WIEMER, G., MOERNAUT, J. *ET AL.* 2015. The role of sediment composition and behavior under dynamic loading conditions on slope failure initiation: a study of a subaqueous landslide in earthquake-prone South-Central Chile. *International Journal of Earth Sciences*, **104**, 1439–1457.

WILHELM, B., NOMADE, J. *ET AL.* 2016. Quantified sensitivity of small lake sediments to record historic earthquakes: implications for paleoseismology. *Journal of Geophysical Research: Earth Surface*, **121**, 2–16.